Inorganic Chemistry

Article

Structural and Magnetic Studies of Two-Dimensional Solvent-Free Manganese(II) Complexes Prepared Via Ligand Exchange Reaction Under Solvothermal Conditions

Shengming Liu,[†] M. T. Bremer,[†] John Lovaasen,[†] A. N. Caruso,[‡] Kevin O'Neill,[§] Lin Simpson,[§] Philip A. Parilla,[§] Michael J. Heben,[§] and Douglas L. Schulz*,[†]

Center for Nanoscale Science and Engineering, North Dakota State University, 1805 NDSU Research Park Drive, Fargo, North Dakota 58102, Department of Physics, University of Missouri—Kansas City, Kansas City, Missouri 64110, and National Renewable Energy Laboratory, 1617 Cole Blvd., Golden, Colorado 80401

Systematic investigation of the ligand exchange reactions between manganese(II) acetate and benzoic acid under solvothermal conditions led to the isolation of crystalline complexes $\{Mn_5(OC(O)CH_3)_6(OC(O)C_6H_5)_4\}_\infty$ (**1**) and $\{Mn_5(OC(O)CH_3)_4(OC(O)C_6H_5)_6\}_\infty$ (**2**) in high (i.e., >90%) yields. The complexes are characterized structurally as 2-D honeycomb-like sheets comprised of edge-shared Mn_{12} loops with some noteworthy differences as follows. First, buckling of the 2-D sheet in **1** is not observed for **2**, presumably as a consequence of additional intersheet phenyl groups in the latter. Second, complex **1** is comprised of only six-coordinate Mn(II), while **2** has both pseudo-octahedral and distorted trigonal bipyramidal coordinate metal ions. Third, while complex **2** exhibits π-stacking interactions with intersheet phenyl–phenyl contacts of 3.285 and 3.369 Å, **1** exhibits no such bonding. Antiferromagnetic exchange is observed with Weiss constants (θ) of −28 and −56 K and Neel temperatures of 2.2 and 8.2 K for complexes **1** and **2**, respectively. The paramagnetic transition at higher temperatures for complex **2** may be attributed to $\pi-\pi$ exchange through phenyl groups in adjacent layers. Preliminary gas sorption studies (76 K) indicate preferential adsorption of H_2 versus N_2 for complex **1** only.

1. Introduction

Manganese carboxylate chemistry is quite diverse given the multiple valence states afforded by the metal center and the various bridging modes offered by the ligand class. The discovery that $[Mn_{12}O_{12}(OC(O)CH_3)_{16}(H_2O)_4]$ clusters are single-molecule magnets provided the basis for probing new zero-dimensional magnetic memory.[1] More recently, interesting magnetic properties have been reported for various Mn(II) carboxylate complexes that are two-dimesional (2-D) and three-dimensional (3-D). For instance, the coordi-

nation polymers $[Mn_3(4\text{-aba})_6]_n$[2a] and $[Mn_3(OH)_2Na_2(3\text{-cnba})_6]_n$[2b] (where aba and cnba are 4-aminobenzoate and 3-cyanobenzoate, respectively) behave as 3-D metamagnets comprised of homometallic ferromagnetic chains with the spin moments linked by interactions in antiferromagnetic (AF)−AF−ferromagnetic (F) and AF−F−AF arrangements, respectively. By way of comparison, $[Mn(3\text{-aba})_2]_n$ adapts a 2-D structure with only weak antiferromagnetic exchange interactions between Mn(II) metal centers.[2c] Complexes $[Mn(3,4\text{-pyda})]$ and $[Mn_3(OH)_2(3,4\text{-pyda})_2(H_2O)_2]$ (where pyda is 3,4-pyridinedicarboxylate) also exhibit antiferromagnetic coupling but adopt a 3-D structure.[3]

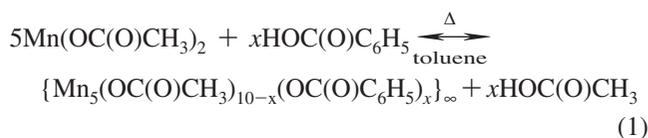We have previously reported new carboxylate chemistry based upon the ligand exchange reaction of Mn(II) acetate with

(1) (a) Sessoli, R.; Tsai, H.-L.; Schake, A. R.; Wang, S.; Vincent, J. B.; Folting, K.; Gatteschi, D.; Christou, G.; Hendrickson, D. N. *J. Am. Chem. Soc.* **1993**, *115*, 1804. (b) Sessoli, R.; Gatteschi, D.; Caneschi, A.; Novak, M. A. *Nature* **1993**, *365*, 141. (c) Aubin, S. M. J.; Wemple, M. W.; Adams, D. M.; Tsai, H.-L.; Christou, G.; Hendrickson, D. N. *J. Am. Chem. Soc.* **1996**, *118*, 7746.

(2) (a) Wang, R.; Gao, E.; Hong, M.; Gao, S.; Luo, J.; Lin, Z.; Han, L.; Cao, R. *Inorg. Chem.* **2003**, *42*, 5486. (b) Li, J.; Tao, J.; Huang, R.; Zheng, L.; Yuen, T.; Lin, C. L.; Varughese, P; Li, J. *Inorg. Chem.* **2005**, *44*, 4448. (c) Wang, R.; Yuan, D.; Jiang, F.; Han, L.; Gao, S.; Hong, M *Eur. J. Inorg. Chem.* **2006**, 1649.

(3) Tong, M.; Wang, J.; Hu, S. *J. Solid State Chem.* **2005**, *178*, 1518.

benzoic acid.[4] In our approach, only noncoordinating species (e.g., toluene) are used, thus avoiding the formation of solvent-containing adducts (e.g., $[Mn_4(OC(O)CH_3)_8(MeOH)_2]_n$[5]) where such moieties have the possibility of blocking pathways for magnetic interactions. In addition, such complexes tend to reorganize structurally upon loss of the solvent molecules, which may limit the application of these materials. While crystalline materials of similar composition can be prepared via an azeotropic flask reaction, solvothermal conditions were employed to produce single crystals of suitable quality for structural determination. In our previous studies, crystals of $\{Mn_5(OC(O)CH_3)_6(OC(O)C_6H_5)_4\}_\infty$ (**1**) were isolated in high yield and shown to have a unique 2-D sheet structure with edge-shared Mn_{12} loops as the basic repeating unit.[4b]

The ligand exchange reaction of $Mn(OAc)_2$ and benzoic acid generates $Mn_5(OAc)_{10-x}(OBz)_x$ ($x = 4$ and 6) where OAc and OBz are abbreviations for acetate and benzoate, respectively. The chemical reaction for this equilibrium is given as eq 1. A systematic exploration of the experimental conditions (e.g., solvothermal reaction temperature, reagent concentration, etc.) was performed, and the magnetic properties of the products were correlated to the chemical composition. In this paper, we report the relationships between the structures of **1** ($x = 4$) and **2** ($x = 6$) and their magnetic properties.

$$5Mn(OC(O)CH_3)_2 + xHOC(O)C_6H_5 \underset{toluene}{\overset{\Delta}{\rightleftarrows}}$$

$$\{Mn_5(OC(O)CH_3)_{10-x}(OC(O)C_6H_5)_x\}_\infty + xHOC(O)CH_3$$

$$(1)$$

2. Experimental Section

Materials and General. All manipulations were performed under N_2 gas using standard Schlenk techniques. Dried, deoxygenated toluene was collected from an Innovative Technologies solvent treatment system and degassed with N_2 for 10 min prior to introduction into an Innovative Technologies N_2-filled glovebox. Anhydrous Mn(acetate)$_2$ (98%) and benzoic acid (99.5%) were used as-received from Aldrich. PTFE-lined Parr autoclave reactors (120 mL) were placed inside the glovebox where the solvent and reagents were loaded. Solvothermal treatments were realized by placing the autoclaves into a temperature-controlled (Omega CN9600) drying oven.

Caution! *Reaction conditions are above the flash point of toluene, and appropriate consideration should be made to safely manage thermal runaway and reactor rupture.*

Preparation of $\{Mn_5(OC(O)CH_3)_6(OC(O)C_6H_5)_4\}_\infty$ **(1).** Compound **1** was prepared as previously reported.[4b]

Preparation of $\{Mn_5(OC(O)CH_3)_4(OC(O)C_6H_5)_6\}_\infty$ **(2).** Mn(OAc)$_2$ (0.400 g, 2.31 mmol), benzoic acid (1.270 g, 10.4 mmol), and toluene (3.5 mL) were loaded into a PTFE-lined Parr autoclave. The Parr reactor was heated from room temperature to 140 °C over a 6 h period and then soaked at 140 °C for 36 h prior to cooling to 30 °C at ~2 °C/h. After cooling, the Parr reactor was returned to the glovebox where a colorless product was isolated. X-ray-

Table 1. Comparison of Crystal Data and Structure Refinement for **1** and **2**

	1	**2**
empirical formula	$C_{40}H_{38}Mn_5O_{20}$	$C_{50}H_{42}Mn_5O_{20}$
formula weight	1113.40	1237.54
cryst syst	orthorhombic	monoclinic
space group	$Aba2$ (41)	$P2(1)/c$
a, Å	19.643(4)	23.664(5)
b, Å	24.014(5)	21.403(4)
c, Å	10.173(2)	10.324(2)
β		92.02(3)
vol, Å^3	4798.6(16)	5225.6(18)
Z	4	4
D (calcd), mg/m^3	1.541	1.573
color of cryst	colorless	colorless
cryst size, mm	0.23 × 0.15 × 0.03	0.31 × 0.27 × 0.12
T, °C	−123	−123
radiation (λ, Å´)	Mo Kα (0.71073)	Mo Kα (0.71073)
μ, mm^{-1}	1.353	1.252
max. and min. transmission	0.9605 and 0.7460	0.8643 and 0.6976
scan mode	ω at 55/−55	ω at 55/−55
2θ limits, deg	3.98−50.04	2.56−54.98
$\pm h$	23	30
$\pm k$	28	−27, 22
$\pm l$	12	13
no. of rflns measd	8182	21455
no. of unique reflns	4176	11985
restraints	7	0
no. of variables	323	676
R_1 [I > 2σ (I)]	0.0599	0.0324
wR_2 (all data)	0.1538	0.1170
R_{int}	0.0386	0.0219
GOF	1.055	1.101

diffraction-quality crystals were stored under Fomblin oil while samples for chemical analysis and magnetic measurements were washed with 3 × 5 mL aliquots of dry toluene and then dried under a vacuum. The yield for this reaction was 0.572 g (>95% based on total Mn). Mp.: 253−255 °C (dec). Anal. Calcd (found) for **2**, $C_{50}H_{42}Mn_5O_{20}$: C, 48.52 (48.25), H, 3.42 (3.46). Selected IR data (KBr, cm^{-1}): 3061 (m), 3029 (w), 2934 (vw), 1593(s), 1559 (s, sh), 1575 (s, sh), 1537 (s), 1494 (w, sh), 1412 (vs), 1345 (m), 1309 (w), 1181 (w), 1157 (w), 1070 (vw), 1024 (m), 948 (w), 856 (w), 838 (w), 822 (vw), 721 (s), 688 (w, sh), 674 (m), 610 (w), 564 (w), 508 (vw), 438 (w).

Single-Crystal Structure Determination. Colorless crystals of complexes **1** and **2** were analyzed using a Nonius Kappa CCD diffractometer with a graphite monochromator and Mo Kα radiation (0.71073 Å) with data collection parameters listed in Table 1. An absorption correction by integration was applied using measured indexed crystal faces as the basis. The structures were solved by the Direct Methods procedures in SHELX97[6] and refined using full-matrix least-squares. Nonhydrogen atoms were refined anisotropically, whereas the hydrogen atoms were placed in ideal, calculated positions with isotropic thermal parameters residing on their respective carbon atoms.

Elemental Analysis. Elemental CH analyses were performed on-site with a LECO CHNS-932 analyzer calibrated against sulfamethazine and ethylenediamine tetracetic acid. Unknown Mn(II) carboxylate samples were ground into a fine powder and loaded into silver capsules inside the drybox with each sample analyzed in triplicate to ensure an accurate determination.

Magnetic Measurements. Thermomagnetic studies were completed with a Quantum Design Physical Properties Measurement System using the vibrating sample magnetometer (VSM) and ACMS options for measurement of the magnetization (M) and

(4) (a) Bremer, M.; Sandstrom, J.; Jeppson, P.; Anderson, B.; Kaderbhai, M.; Kizilkaya, O.; Zinoveva, S.; Liu, S.; Schulz, D. L.; Caruso, A. N. *Polyhedron* **2007**, *26*, 2110. (b) Liu, S.; Caruso, A. N.; Jeppson, P.; Sandstrom, J.; Schulz, D. L. *Polyhedron* **2007**, *26*, 2235.

(5) Tasiopoulos, A. J.; Harden, N. C.; Abboud, K. A.; Christou, G. *Polyhedron* **2003**, *22*, 133.

(6) Sheldrick, G. M. *SHELX 97*; University of Göttingen: Göttingen, Germany, 1997.
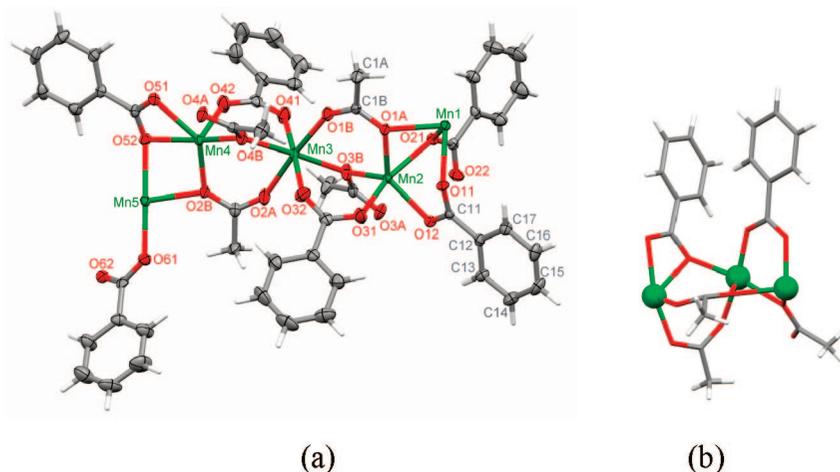
Figure 1. (a) The ORTEP view of the asymmetric unit of complex **2** at the 70% probability level. H atoms are drawn as sticks for clarity. (b) Asymmetric unit of **1** in ball and stick.

susceptibility (χ) as a function of applied field (H) and temperature (T). All studies were performed on powder samples that were loaded, transferred, and measured under inert conditions (i.e., <1 ppm H_2O and O_2). VSM sample holders were provided by Quantum Design, and pharmaceutical gel caps sealed with Kapton tape were used for ACMS measurements (data corrected for diamagnetic background). For temperature-dependent measurements, samples were cooled in a magnetic field of less than 0.05 Oe (i.e., zero-field cooled) with data collection realized during warmup. The ac susceptibility measurements utilized $H_{dc} = 0$ and $H_{ac} = 3$ Oe at ν = 9973 Hz with VSM and ACMS calibrated with DyO and Pd standards.

Gas Sorption. Colorless powders (i.e., 35.1804 mg of complex **1** and 81.1975 mg of **2**) were loaded into quartz tubes with a metal/quartz junction and a VCR connection. A metal-sealed valve that was mated with the quartz tube permitted control of the composition of the atmosphere over the sample during subsequent handling. The sample tubes were connected to a turbomolecular-pumped vacuum station equipped with a mass spectrometer. The samples were degassed by heating to 150 °C at 1°/s under a dynamic vacuum. Mass spectrometry indicated the evolution of atmospheric gases (e.g., CO_2, N_2, and H_2O) for **1** and **2** during the initial degassing cycle. After cooling to room temperature, the valve was closed and the sample was transferred to the Sieverts apparatus under a vacuum. After cooling to 76 K under a dynamic vacuum, H_2 adsorption data were collected by exposing the sample to increasing gas pressures from 10 to 800 Torr. The hydrogen gas was purified at the point of use by activated molecular sieves. N_2 adsorption data were collected in a similar fashion following an intermediate 150 °C degassing step *in situ*. The nitrogen gas is expected to be very pure as it was obtained from boil-off from the liquid.

Other Measurements. A Bruker FT-IR Vertex 70 spectrophotometer was used to collect infrared spectra of the products (KBr pellets). Sealed capillary melting points were determined with an Electrothermal melting point apparatus.

3. Results and Discussion

Structural Aspects. A comparison of crystal data and structural refinements for complexes **1** and **2** is given in Table 1. Complex **1** crystallizes as hexagonal thin plates (less than 0.03 mm), while **2** exists as hexagonal blocks. The asymmetric unit for **2** (i.e., $Mn_5(OAc)_4(OBz)_6$) is similar to twice the asymmetric unit for **1** (i.e., $Mn_5(OAc)_6(OBz)_4$), as shown
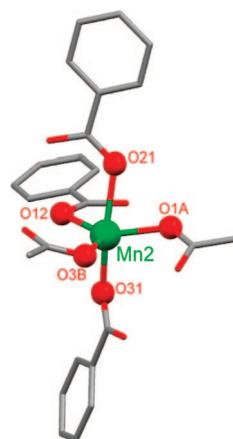

Figure 2. Coordination environment of Mn2 in **2**.

in Figure 1. The structures differ mainly in the metal-to-ligand ratio (Mn/OAc/OBz), with 5:6:4 for **1** and 5:4:6 for **2**. While the three Mn atoms in **1** are in pseudo-octahedral geometry, the Mn2 atom in complex **2** is five-coordinate (Figure 2) with Mn1, Mn3, Mn4, and Mn5 in 6-fold coordination. The geometry of five-coordinate metals may be described in terms of the τ factor where $\tau = 0$ represents square pyramidal and $\tau = 1$ trigonal bipyramidal.[7] The angular parameter for Mn2 in **2** suggests a structural geometry intermediate between trigonal bipyramidal and square pyramidal with $\tau = (\beta - \alpha)/60 = (162.03 - 131.30)/60 = 0.51$ (where $\beta = $ O21−Mn2−O31 and $\alpha = $ O12−Mn2−O1A).

The Mn−Mn distances in complex **1** are 3.317, 3.405, and 3.398 Å—typical for manganese carboxylate systems. However, complex **2** has two relatively short metal−metal distances (i.e., Mn1−Mn2 = 3.1025 Å and Mn4−Mn5 = 3.1302 Å) with the remaining Mn−Mn distances being relatively longer (i.e., 3.406, 3.490, 3.503, and 3.533 Å). While density functional theory calculations and electron paramagnetic resonance studies would help elucidate the nature of the 5-fold coordination, it appears the close

(7) (a) Addison, A. W.; Rao, T. N.; Reedijk, J.; van Rijn, J.; Verschoor, G. C. *J. Chem. Soc., Dalton Trans.* **1984**, 1349. (b) Alvarez, S.; Llunell, M. *J. Chem. Soc., Dalton Trans.* **2000**, 3288.
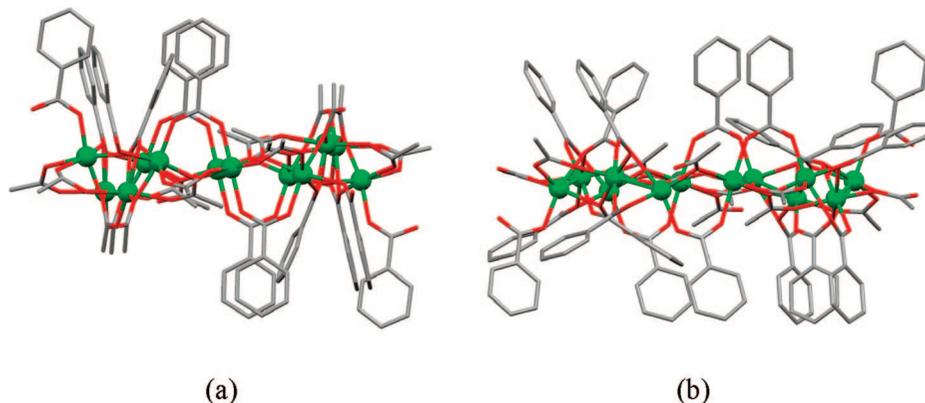
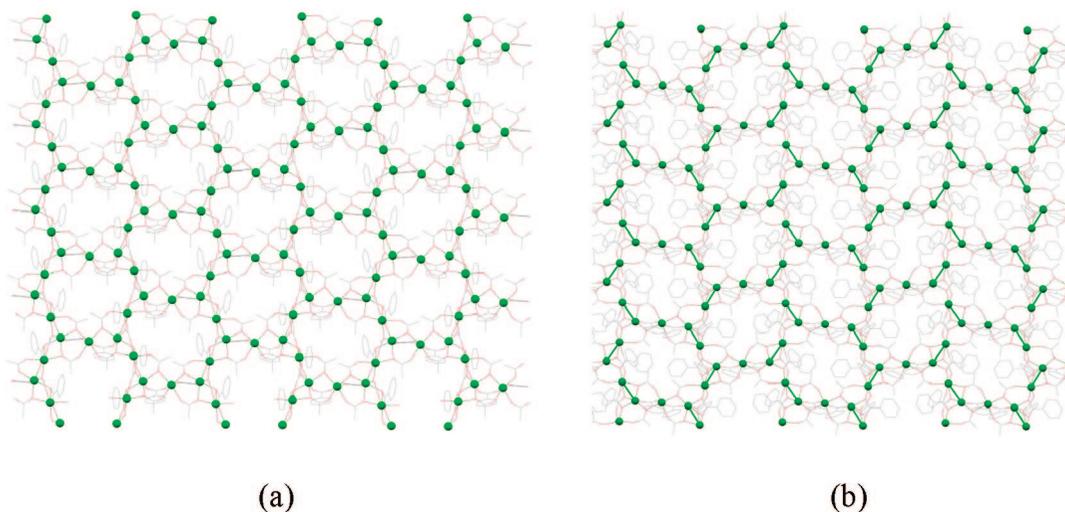**Figure 3.** Cross-section view of Mn$_{12}$ loops of (a) **1** and (b) **2**.

Figure 4. 2-D sheets of (a) **1** and (b) **2**. Mn atoms are drawn as green balls, while carbon and oxygen atoms are drawn as grey and red wire frames, respectively. Hydrogen atoms are omitted for clarity.

metal−metal interaction (i.e., Mn1−Mn2) allows such a distortion from the normally observed pseudo-octahedral geometry. It is noteworthy that the Mn1−Mn2 and Mn4−Mn5 distances in complex **2** appear to be the shortest known for Mn(II) carboxylates. However, other manganese complexes exhibit similar or even shorter distances as follows: 3.181 Å in [Mn$_6$(O)$_2$Piv$_{10}$],[8] 3.001 Å in MnHPO$_3$,[9a] 2.946 Å in MnHPO$_3$,[9b] 2.999 Å in MnHPO$_3$,[9c] 3.099 Å in Mn$_3${C$_6$H$_3$-(CO$_2$)$_3$-1,3,5}$_2$],[10] and 2.88 Å for Mn$^{III}_4$O$_2$-related complexes.[11]

For both complexes **1** and **2**, extension of the asymmetric unit gives Mn$_{12}$ loops that may be further expanded into 2-D sheets. For **1**, there are 12 manganese atoms, 18 acetates, and 12 benzoates in each loop which may be represented as Mn$_{12}$(OAc)$_{18}$(OBz)$_{12}$. As shown in Figure 3a, the 12 benzoate ligands of **1** and six acetates are located on axial positions, with the remaining 12 acetates in equatorial positions. For
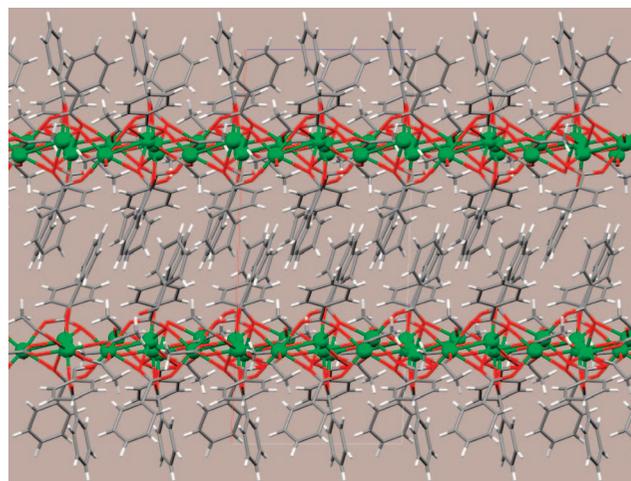
(8) Ovcharenko, V.; Fursova, E.; Romanenko, G.; Ikorskii, V. *Inorg. Chem.* **2004**, *43*, 3332.
(9) (a) Fernandez, S.; Pizarro, J. L.; Mesa, J. L.; Lezama, L.; Arrioitua, M. I.; Olazcuaga, R.; Rojo, T. *Inorg. Chem.* **2001**, *40*, 3476. (b) Fernandez-Armas, S.; Mesa, J. L.; Pizarro, J. L.; Pena, A.; Chapman, J. P.; Arrioitua, M. I. *Mater. Res. Bull.* **2004**, *39*, 1779. (c) Fernandez, S.; Mesa, J. L.; Pizarro, J. L.; Lazama, L.; Arrioitua, M. I.; Olazcuaga, R.; Rojo, T. *Chem. Mater.* **2000**, *12*, 2092.
(10) Gutschke, S. O. H.; Molinier, M.; Powell, A. K.; Winpenny, E. P.; Wood, P. T. *Chem. Commun.* **1996**, 823.
(11) Wang, S.; Tsai, H.-L.; Folting, K.; Martin, J. D.; Hendrickson, D. N.; Christou, G. *Chem. Commun.* **1994**, 671.
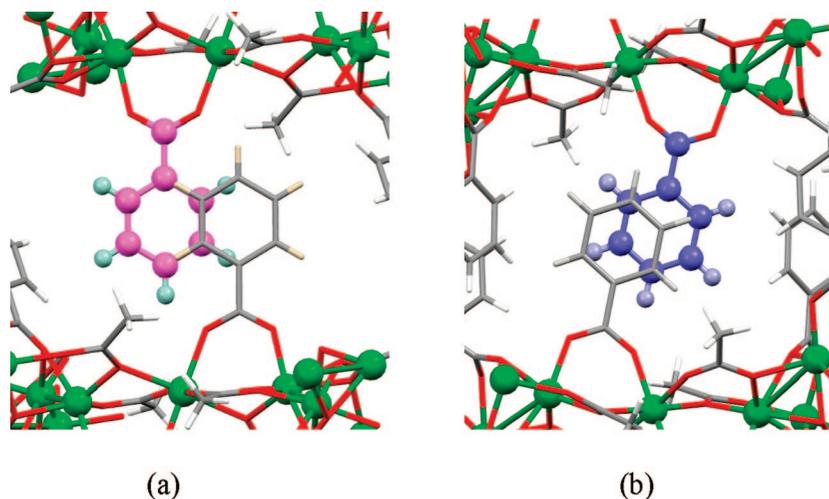
Figure 5. (a) Cross-section view down *b* axis illustrating planar stacking. Manganese atoms are drawn as green balls, while oxygen, carbon, and hydrogen atoms are drawn as red, grey, and white wires, respectively.

complex **2**, all benzoate ligands are on axial positions with nine above the loop plane and the other nine below the loop, while all 12 acetate ligands lie in the equatorial plane (Figure 3b). These observations teach that 18 ligands in the axial position and 12 in the equatorial is the lowest energy conformation for this 2-D Mn(II) carboxylate system.

Figure 6. Zoom-in views showing $\pi-\pi$ interactions of adjacent layers in **2** with a spacing of (a) 3.285 Å and (b) 3.369 Å. Carbon and hydrogen atoms at the lower layers are drawn as different colors for clarity.
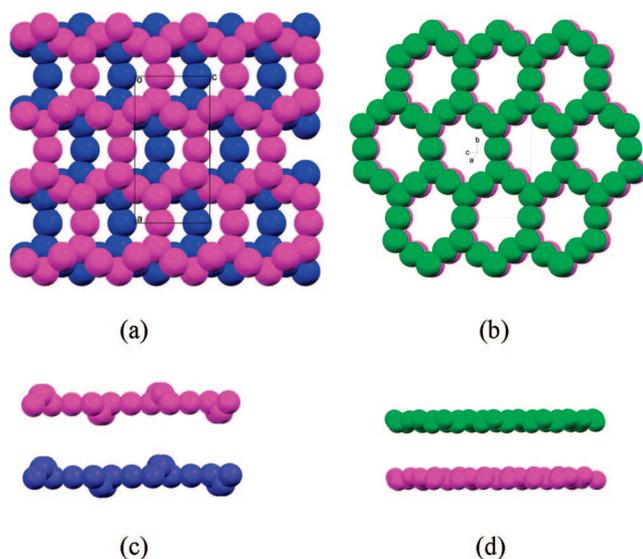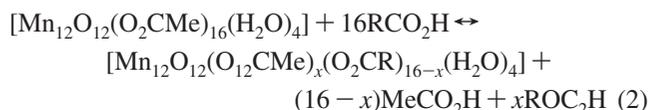

Figure 7. Spacefill packing diagrams of Mn atoms showing (a) ABAB packing in **1** (viewed perpendicular to the 2-D sheet), (b) AAAA packing in **2** (viewed perpendicular to the 2-D sheet), (c) a slight buckling of the 2-D sheet for **1**, and (d) a relatively flat 2-D sheet for **2**. Ligand molecules are omitted for clarity.

The two-dimensional sheet structures (*vide supra*) are generated through symmetric operations and are shown in Figure 4. From this view, the acetate-to-benzoate ratios for **1** (Figure 4a) and **2** (Figure 4b) are only subtly differentiable. Each Mn$_{12}$ loop in **2** has the four short Mn–Mn distances (i.e., Mn1–Mn2 and Mn4–Mn5) shown as green "connections" to help identify these interactions in the extended structure (Figure 4b). When viewing the 2-D structure of **2** in cross-section (Figure 5), edge-to-edge (Figure 6a) and offset (Figure 6b) π interactions are observed with distances of 3.285 and 3.369 Å, respectively. The angles between the phenyl ring plane and the Mn$_{12}$ loop plane are 82 °(Figure 6a) and 67° (Figure 6b). These $\pi-\pi$ interaction distances are shorter than those reported for [Mn(OMe)(O$_2$CPh)]$_n$ (i.e., 3.719 Å)[12] and [Mn$_4$O$_2$(O$_2$CCH$_3$)$_4$(O$_3$PC$_6$H$_{11}$)$_2$(phen)$_2$] (i.e., 3.567 Å)[13] yet similar to those for Mn$_3$(OAc)$_6$(bpy)$_2$ (i.e., 3.325 Å).[14]

An interesting Mn$_{12}$ loop structure is revealed when the acetate and benzoate ligands are omitted, as illustrated by spacefill packing diagrams of Mn atoms (Figure 7). The stacking of the Mn$_{12}$ plane in **1** is quite similar to graphite with an ABAB motif (Figure 7a). The same perspective of **2** (Figure 7b) shows the Mn$_{12}$ loops are aligned on top of one another in an AAAA pattern. A similar change from ABAB to AAAA has been observed for graphite when the interplanar distance is increased by intercalating atoms such as lithium.[15] For the present study, the additional axial benzoate ligands in **1** versus **2** serve to increase the interlayer distance with a concomitant change from ABAB to AAAA. Additionally, the cross-section view of two adjacent layers of complex **1** shows buckling (Figure 7c), while that for **2** reveals relatively flat sheets (Figure 7d).

Synthetic Aspects. It was previously reported by Christou et al. that carboxylate exchange in Mn$_{12}$ clusters occurs according to an equilibrium reaction (eq 2).[16] Isolation of the end member products was realized by one of the following two methods: (i) the azeotropic removal of acetic acid (i.e., CH$_3$CO$_2$H-toluene), thus driving the equilibrium of eq 2 to the right, or (ii) isolation of the incompletely exchanged product followed by additional treatment with excess carboxylic acid.[16b]

$$[Mn_{12}O_{12}(O_2CMe)_{16}(H_2O)_4] + 16RCO_2H \leftrightarrow$$
$$[Mn_{12}O_{12}(O_{12}CMe)_x(O_2CR)_{16-x}(H_2O)_4] +$$
$$(16 - x)MeCO_2H + xROC_2H \quad (2)$$

A similar approach was employed in our Mn(II) studies with equilibrium products initially isolated and characterized

(12) (a) Tasiopoulos, A. J.; Wernsdorfer, W.; Abbound, K. A.; Christou, G. *Inorg. Chem.* **2005**, *44*, 6324. (b) Tasiopoulos, A. J.; Wernsdorfer, W.; Abbound, K. A.; Christou, G. *Polyhedron* **2005**, *24*, 2505.
(13) Ma, Y.-S.; Yao, H.-C; Hua, W.-J.; Li, S.-H; Li, Y.-Z.; Zheng, L.-M. *Inorg. Chim. Acta* **2007**, *360*, 1645.
(14) Ménage, S.; Vitols, S. E.; Bergerat, P.; Codjovi, E.; Kahn, O.; Girerd, J.-J.; Guillot, M.; Solans, X.; Calvet, T. *Inorg. Chem.* **1991**, *30*, 2666.
(15) Song, M. K.; Hong, S. D.; No, K. T. *J. Electrochem. Soc.* **2001**, *148*, A1159.
(16) (a) Soler, M.; Artus, P.; Folting, K.; Huffman, J. C.; Hendrickson, D. N.; Christou, G. *Inorg. Chem.* **2001**, *40*, 4902. (b) Eppley, H. J.; Tsai, H.-L.; de Vries, N.; Folting, K.; Christou, G.; Hendrickson, D. N. *J. Am. Chem. Soc.* **1995**, *117*, 301.
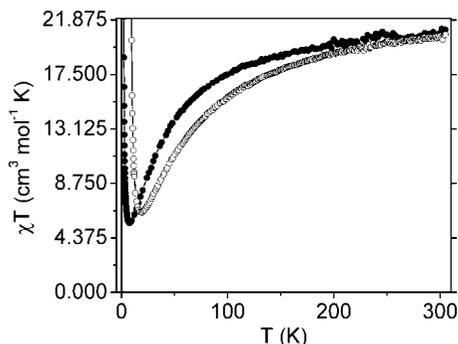
Figure 8. Susceptibility−temperature product, χT, for complexes **1** (closed circles) and **2** (open circles) below 305 K. Data for both samples are indicative of a ferrimagnetic material, with complex **2** showing a lower Weiss constant ($\theta = -56$ K) than **1** ($\theta = -26$ K).

Figure 9. $M(T)$ (top), $\chi T(T)$ (middle), and the out-of-phase component of ac susceptibility, $\chi''(T)$ (bottom), for complexes **1** (open circles) and **2** (closed circles) below 11 K. The spikes in χT suggest a magnetic phase transition that coincides with the appearance of a finite χ'' and a remnant moment.

as, for example, $Mn_5(OAc)_6(OBz)_4$. These products were then further reacted with excess benzoic acid in an attempt to isolate the $Mn(OBz)_2$ end-member (eq 2). While $Mn(OBz)_2$ has been previously observed,[17] further reaction of isolated materials (e.g., $Mn_5(OAc)_6(OBz)_4$) did not yield products that showed evidence of marked additional ligand exchange. This variance from the previous reports may be a consequence of differences in solubility where no loosely bound coordinating molecules (e.g., ethanol and water) are available to promote dissolution of the manganese carboxylates or solution-phase ligand exchange. As an aside, solvothermal reaction of $Mn(OAc)_2$ with 10 mol equiv of benzoic acid gave a product with a final chemical composition of $Mn_5(OAc)_{0.7}(OBz)_{9.3}$.

Magnetic Properties. Both complexes were characterized as a function of applied field and temperature. Figure 8 shows the susceptibility−temperature product, χT, of **1** and **2**. χT has a value of 21.1 and 20.3 cm³ mol⁻¹ K at 305 K for **1** and **2**, respectively. This is lower than the 21.875 cm³ mol⁻¹ K value expected for five individually isolated Mn(II) metal centers. χT decreases with decreasing temperature (although **2** drops faster than **1**), reaching a broad minimum of 5.6 cm³ mol⁻¹ K at 7.8 K and 6.4 cm³ mol⁻¹ K at 19.1 K for **1** and **2**, respectively. Not only the reduced χT magnitude but also the negative slope and the negative Weiss constants (from the χ^{-1} intercept) are indicative of antiferromagnetic exchange. As the temperature is further reduced, a dramatic increase in the value of χT and its slope occurs for both complexes, suggesting an increase in effective moment despite antiferromagnetic exchange. The appearance of an out-of-phase component in the ac susceptibility, $\chi''(T)$, as well as remnant magnetization at 2.2 K and 8.2 K for complexes **1** and **2**, respectively, coincides with this spike in χT and marks the onset of a spontaneous moment and the proposed ferrimagnetic long-range order (Fig. 9).

The appearance of ferrimagnetism in a homometallic material is quite unusual, and the few examples that exist often require ferromagnetic as well as antiferromagnetic
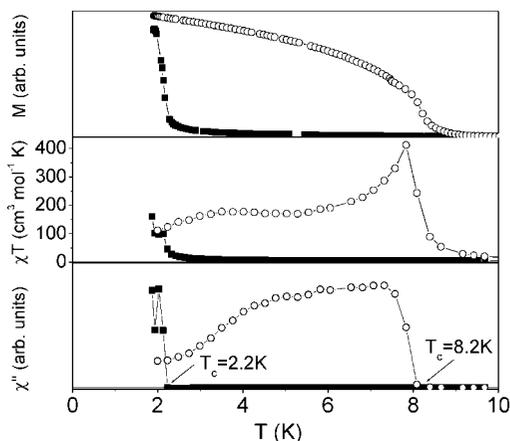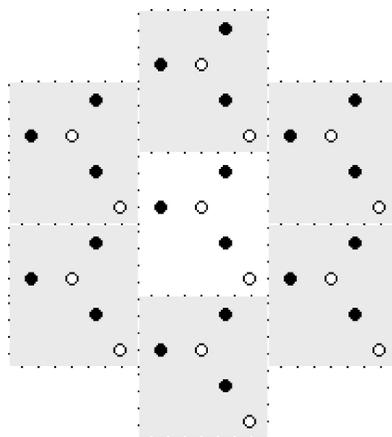

Figure 10. A highlighted unit cell of the 12-member honeycomb lattice. Closed and open circles represent distinct magnetic sites; antiparallel alignment of adjacent spins leaves one spin uncompensated, resulting in ferrimagnetism.

exchange.[18] However, with close inspection, one can see that ferrimagnetism is intrinsic to the 12-member honeycomb lattice with purely antiferromagnetic exchange; that is, a geometrically induced moment. Reducing this ideal lattice to a magnetic unit cell produces a five-member unit (Figure 10), and the antiparallel alignment of adjacent magnetic centers leaves one of the five magnetic moments uncompensated. It should be noted that both **1** and **2** deviate somewhat from ideal 12-member honeycombs in that the local polygon is not perfectly planar and the oxalate bridging between magnetic centers is not symmetric, although the essential topological pathways exist. Indeed, data from the attempted saturation at 2 K (Figure 11) are consistent with the above description. The complexes appear to saturate near a value of 5 μ_B/formula unit (1/5 the total moment) before

(17) Manson, J. L.; Schlueter, J. A. Personal communication, August 17, 2006.

(18) (a) Gao, E. Q.; Yue, Y. F.; Bai, S. Q.; He, Z.; Yan, C. H. *J. Am. Chem. Soc.* **2004**, *126*, 1419. (b) Reis, M. S.; Moreira dos Santos, A.; Amaral, V. S.; Brandão, P.; Rocha, J. *Phys. Rev. B: Condens. Matter Mater. Phys.* **2006**, *73*, 214415. (c) Ghosh, A. K.; Ghoshal, D.; Zangrando, E.; Ribas, J.; Chaudhuri, N. R. *Inorg. Chem.* **2005**, *44*, 1786. (d) Li, J.-T.; Tao, J.; Huang, R.-B.; Zheng, L.-S.; Yuen, T.; Lin, C. L.; Varughese, P.; Li, J. *Inorg. Chem. Commun.* **2005**, *44*, 4448. (e) Konar, S.; Mukherjee, P. S.; Zangrando, E.; Lloret, F.; Chaudhuri, N. R. *Angew. Chem., Int. Ed.* **2002**, *41*, 1561.
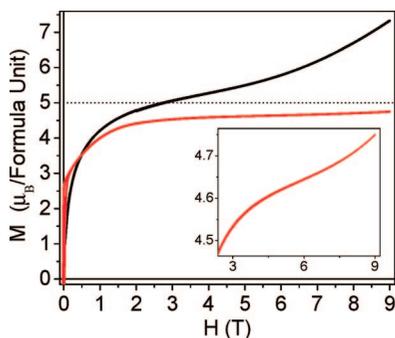
Figure 11. $M(H)$ at 2 K for complex **1** (black) and complex **2** (red). Both magnetizations have an inflection point above $3T$. The inset shows magnification of **2**, highlighting the transition.

higher fields (>3 T) induce a transition toward parallel alignment and the magnetization inflects and approaches a higher saturation value, presumably 25 μ_B at fields much greater than 9 T. Supporting this description is the observation and theoretical treatment of an analogous transition in the trinuclear molecule $Mn^{II}_3(CH_3CO_2)_6(bpy)_2$, featuring similar acetato bridging to that of **1** and **2** in which high fields at low temperatures increased the moment beyond the 5 μ_B anticipated for antiferromagnetic alignment.[14] The magnetization of complex **2** falls short of 5 μ_B, where the small deviation could be the result of spin canting, sample weighing error, a small spin–orbit quenching that tracks with the magnetocrystalline anisotropy and distorted octahedra,[4a] or anisotropy from the single five-coordinate Mn that is not present in **1**.

While intralayer structural similarities produce the same essential behavior in both samples, there are marked differences in the Weiss temperature and ordering temperatures that may be the results of interlayer exchange and changes in intralayer bridging. Complex **2** has a much lower Weiss temperature ($\theta = -56$ K) than complex **1** ($\theta = -28$ K). A material that was chemically characterized as "$Mn_5(OAc)_5$-$(OBz)_5$" showed a Weiss constant of -44 K (i.e., nearly halfway between complex **1** and **2**). Powder X-ray diffraction of the "$Mn_5(OAc)_5(OBz)_5$" sample shows a 1:1 mixture of **1** and **2**. Similar magnetic behavior has been previously identified for $Fe_{1-x}Mn_xCl_2 \cdot 2H_2O$ mixtures.[19]

It is known that lower Weiss constants are indicative of stronger antiferromagnetic exchange when considering complexes with similar arrangements of magnetic species.[20] Furthermore, the χT of **2** decreases faster with decreasing temperature than **1**, indicating a greater tendency of neighboring spins to align antiparallel. The stronger intralayer exchange could be due to small changes in bridging ligands, or perhaps direct exchange between certain Mn(II) ions suggested by the short interior distances (e.g., Mn1–Mn2 = 3.1026 Å, Mn4–Mn5 = 3.1303 Å). Further evidence of a deviation in intralayer exchange strength is demonstrated in Figure 11, wherein **2** quickly approaches the initial saturation value and only begins its high-field transition toward parallel
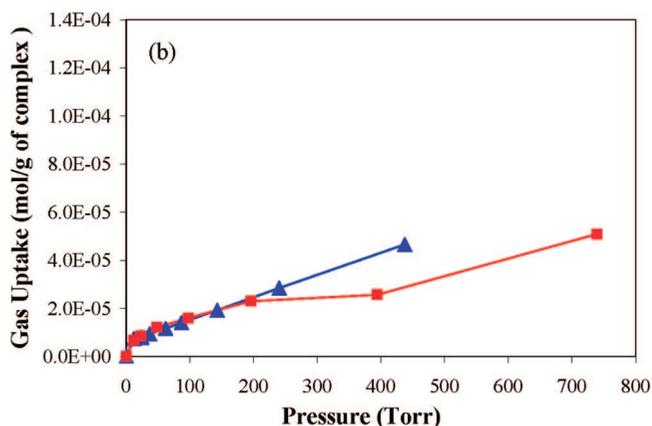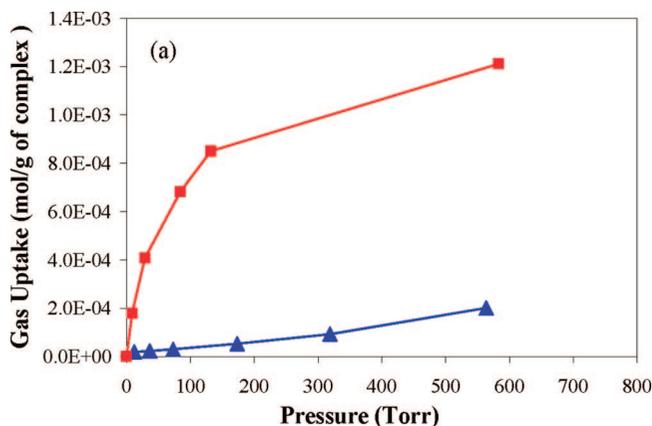

Figure 12. Sieverts data at 76 K for (a) complex **1** and (b) complex **2** showing equilibrium amounts of sorbed gas. Data for H_2 and N_2 adsorption are shown as red squares and blue triangles, respectively. Note the difference in scale between a and b.

alignment near $9T$, while complex **1** barely begins the initial saturation before entering this field-induced transition.

From Figure 11, it is observed that **2** displays 3-D long-range ferrimagnetic ordering at 8.2 K, which is significantly higher than the 2.2 K observed in **1**. Because interlayer exchange is much weaker than intralayer exchange in these systems, the onset of long-range order may be very sensitive to the strength of this exchange. Shorter interlayer spacing (11.83 vs 12.01 Å) and direct overlap of Mn(II) loops in **2** (Figure 7) could support stronger interlayer exchange than in **1**. However, studies show that changes in interlayer spacing have little effect on the T_c of layered complexes when dipolar interactions are the dominant form of magnetic exchange.[21] Another consideration is the existence of the π–π interactions in **2** (Figure 6) but not in **1**; such structural features have been shown to be a pathway for superexchange[22] that is strongly warrantable relative to dipolar interaction. It should be noted that long-range intralayer spin correlation is thought to stabilize interlayer dipolar interactions;[21] therefore, stronger intralayer exchange in **2** could also substantially increase T_c. Despite the 12 Å spacing, dipolar interactions should still be considered as a coupling

(19) Zenmyo, K,; Kubo, H.; Deguchi, H.; Konishi, K.; Takeda, K. *J. Phys. Soc. Jpn.* **2000**, *69*, 3980.

(20) (a) Cullity, B. L. *Introduction to Magnetic Materials*; Addison-Wesley: Reading, MA, 1972; p 133. (b) Kahn, O. *Molecular Magnetism*; VCH Publishers Inc.: New York, 1993, p 27.

(21) Laget, V.; Hornick, C.; Rabu, P.; Drillon, M.; Ziessel, R. *Coord. Chem. Rev.* **1998**, *178–180*, 1533.

(22) Vazquez, M.; Taglietti, A.; Gatteschi, D.; Sorace, L.; Sangregorio, C.; Gonzalez, A. M.; Maneiro, M.; Pedrido, R. M.; Bermejo, M. R. *Chem. Commun.* **2003**, 1840.

basis since the dipole–dipole exchange goes as the square of the spin where this system has $s = {}^5/_2$.

Gas Sorption. Figure 12 shows the results of the gas adsorption characterization of complexes **1** (Figure 12a) and **2** (Figure 12b). The data for **1** indicate that approximately 6 times more hydrogen than nitrogen is sorbed at the highest pressures. This is remarkable considering the experiments were performed near the boiling point of liquid nitrogen. Evidently, H_2, with a kinetic diameter of 2.8 Å, can access significantly more of the internal surface area in **1** than can N_2 with a kinetic diameter of 3.6 Å. Similar behavior has been noted recently for microporous manganese(II) formate.[23] By way of comparison, **2** shows no difference between the molar amounts of sorbed H_2 and N_2 (Figure 12b), and each of these are a factor of 2 smaller than the amount of N_2 sorbed on **1**. In simple terms, it appears that no internal surface area in **2** is accessible by H_2 species. It is counterintuitive that the ABAB-stacked arrangment of complex **1** (Figure 7a) exhibits H_2 sorption while the zeolite-like (i.e., AAAA stacking) structure observed for **2** (Figure 7b) shows no H_2 uptake. As only the atoms of the metal coordination sphere data are given in Figure 7, it follows that the differences in the ancillary ligation (i.e., benzoate and acetate ligands) lead to the variations of gas sorptive properties in **1** versus **2**. It appears that complex **2** maintains a more-efficiently packed—and conversely less porous—structure where the sorption of H_2 is not favored. The H_2 bonding observed between phenyl groups of neighboring layers in complex **2** (Figure 6) may be a manifestation of a densely packed structure. Future molecular modeling studies utilizing crystallographic data should allow a determination of the effective porosity for **1** and **2**, thus providing evidence that the differences in gas sorption could be attributed to steric effects.

(23) Dybtsev, D. N.; Chun, H.; Yoon, S. H.; Kim, D.; Kim, K. *J. Am. Chem. Soc.* **2004**, *126*, 32.

Conclusions

The two-dimensional solvent-free manganese(II) complexes $\{Mn_5(OC(O)CH_3)_6(OC(O)C_6H_5)_4\}\infty$ (**1**) and $\{Mn_5(OC(O)CH_3)_4(OC(O)C_6H_5)_6\}_\infty$ (**2**) were prepared through ligand exchange reactions under solvothermal conditions in toluene at high yields. Both coordination polymers are comprised of 2-D honeycomb-like sheets with an edge-shared Mn_{12} loop as the repeating unit. In addition to the notable difference in composition (i.e., acetate-to-benzoate ratio of 6:4 in **1** and 4:6 in **2**), the differences in coordination geometry of Mn(II) centers (i.e., three pseudo-octahedral for **1** with one distorted trigonal bipyramidal and four psuedo-octahedral for **2**) and distances between manganese metals are noteworthy. While complex **2** appears to possess π stacking with interlayer phenyl–phenyl contacts of 3.285 and 3.369 Å, complex **1** does not exhibit such interaction. The magnetic susceptibility indicates antiferromagnetic exchange in both complexes with Weiss constants of $\theta = -28$ and -56 K and transition temperatures of $T_c = 2.2$ and 8.2 K for complexes **1** and **2**, respectively. The presence of a remnant moment in this antiferromagnetic homometallic and homovalent system, presumably due to geometrical non-compensation, is unusual especially when defining the mechanism responsible for coercivity. The higher transition temperature of complex **2** may be attributed to interlayer $\pi-\pi$ exchange.

Supporting Information Available: Crystal structure and powder XRD of **1**, **2**, and a sample with the composition of $Mn_5(OC(O)CH_3)_5(OC(O)C_6H_5)_5$. This material is available free of charge via the Internet at http://pubs.acs.org.

IC7020879